RSC Advances

PAPER

View Article Online
View Journal | View Issue

Cite this: *RSC Adv.*, 2015, **5**, 30084

Synthesis of free-standing reduced graphene oxide membranes with different thicknesses and comparison of their electrochemical performance as anodes for lithium-ion batteries

Jinxing Wang and Hui Wang*

Received 26th January 2015
Accepted 23rd March 2015

DOI: 10.1039/c5ra01533b

www.rsc.org/advances

Free-standing reduced graphene oxide membranes (rGOMs) with different thicknesses and carbon contents are prepared *via* a simple, low cost, scalable, and eco-friendly two-step process. Scanning electron microscopy results show that rGOMs thicken with increasing GO solution concentration. The as-prepared free-standing rGOMs are directly used as anode materials for lithium-ion batteries without conducting additives or binders. The cycling performance and rate capability of the membrane electrodes are investigated and compared, and results indicate that not all of the synthesized rGOM anodes exhibit good lithium storage properties. Only those membranes with a coriaceous structure, approximately 2.5 μm thickness, and suitable reduction degree present high performance for reversible lithium storage. Reasons for these findings are also provided.

Introduction

Rechargeable lithium-ion batteries (LIBs) have recently received more attention than other rechargeable cells in portable electronic devices and are regarded as one of the most promising devices for electric-vehicle applications because of their many advantages, which include high energy storage capacity, long cycle life, and environment-friendliness.[1] The energy density and electrochemical performance of LIBs mainly depend on the chemical and physical properties of their cathode and anode materials, hence, a large amount of research has been done to improve the quality of the electrode materials. An ideal electrode material for LIBs must have high lithium storage capability as well as a stable structure for long cyclability.[2,3] Graphite is the most widely used anode material in LIBs because of its reliability, high coulombic efficiency, and good cycling performance. However, in graphitic carbons, lithium can form an intercalation compound LiC_6, which endows graphite with a low theoretical specific capacity of only 372 mA h g^{-1}.[4] Given the limited capacity of graphite, the energy density of LIBs cannot meet the high requirements of portable electronic devices and recently developed fully electric vehicles. To improve the electrochemical performance of LIBs, considerable efforts have been devoted to finding new electrode materials with higher energy density than traditional electrodes and improved battery capacity, cycle life, and charge–discharge rates.[5]

Graphene is an intriguing carbon nanomaterial with the structure of a one-atom thick two-dimensional (2D) sheet of sp^2 hybridized carbon. The extended honeycomb network of graphene is the basic building block of other important allotropes: it can be wrapped to form 0D fullerenes, rolled to form 1D nanotubes, and stacked to form 3D graphite, has attracted special research attention.[6] This material presents unique physical and chemical characteristics, such as superior electrical conductivity, excellent mechanical flexibility, high transmittance, large surface area, and an open and flexible porous structure.[7–11] Graphene has been investigated for a variety of applications, including batteries, electromagnetic devices, supercapacitors, sensors, mechanical resonators, and biomedicines.[12,13] In terms of LIBs, graphene-based electrodes are reported to accommodate lithium more readily than common graphite anodes, this feature may be attributed to additional reaction mechanisms other than intercalation, such as fast lithium adsorption and electron transportation, faradaic capacitance, and defect trapping.[14–16] The reduced graphene oxide (rGO) is a functionalized graphene, reduced from graphene oxide (GO) with various oxygen functional groups, including hydroxyl and carbon–oxygen double bonds (C=O and O–C=O), on the carbon surface. The redox reactions of lithium ions and the surface oxygen functional groups are considered as the primary lithium capturing mechanism in the functionalized carbon electrodes.[17] By avoiding the kinetic limitation imposed by extremely slow solid-state diffusion, the faradaic redox reaction (fast pseudocapacitive surface reaction) can result in high-power performance.[17] rGO materials can also be assembled into free-standing paper-like membranes and applied as

Key Laboratory of Synthetic and Natural Functional Molecule Chemistry (Ministry of Education), College of Chemistry & Materials Science, Northwest University, Xi'an 710069, PR China. E-mail: huiwang@nwu.edu.cn; Fax: +86 29 88303798; Tel: +86 29 88363115

binder-free anodes for LIBs. In contrast to the conventional anode preparation process, the need to use additives and binders can be avoided by employing free-standing membranes with excellent mechanical flexibility/stability.[18,19] The binder-free electrode configuration can further enhance rate capacities by allowing better access to the electrolytes.[20] Free-standing paper-like electrodes are also useful in developing wearable and flexible energy storage devices.[21]

Based on previous findings, the present study focuses on free-standing, binder-free model rGOMs as electrode materials for LIBs. Given that the electronic properties of rGOMs rely heavily on their thickness and reduction degree,[22] the relation between electrochemical performance and rGOMs with various thicknesses and reduction degrees as anodes for LIBs is systematically explored. Herein, six free-standing rGOMs with varying thicknesses are prepared *via* a simple, scalable, and effective two-step fabrication method, which includes vacuum filtration and chemical reduction. The influences of different thicknesses and reduction degrees of rGOMs on their mechanical, optical, and other properties are studied. The electrochemical activities of the rGOM anodes are also evaluated and compared. Investigation results suggest that only those materials with a coriaceous structure and appropriate thickness and reduction degree exhibit high performance for reversible lithium storage. Reasons behind the high electrochemical performance observed are extensively investigated and discussed.

Experimental

Preparation of graphite oxide (GO)

GO was synthesized from natural flake graphite (99%, Qingdao Chenyang graphite Co., Ltd. Product) *via* acid-oxidation according to a modified Hummers method.[23] In a typical synthesis, graphite powder (1 g) was put into the mixed solution of H_2SO_4 (98%, 92 mL) and HNO_3 (65%, 24 mL) while stirring in an ice-water bath as a safety measure to keep the temperature below 10 °C. Then, $KMnO_4$ (6 g) was added to the solution above and the rate of adding was controlled carefully to keep the mixture temperature from exceeding 20 °C. The mixture was kept in the ice-water bath for 2 h and then stirred continuously at 35 °C for half an hour. Next, the temperature of the mixture solution was increased to 85 °C and maintained for 30 min. Subsequently, 92 mL of deionized (DI) water was added slowly to the mixture within 15 min, and the temperature was kept at 85 °C for another 30 min until a brilliant yellow product was obtained. Afterward, the mixture was cooled to room temperature and then diluted with 10 mL of H_2O_2 (30%) to reduce the residual permanganate to soluble manganese ions. Finally, the mixture was washed several times with DI water (1 L) and 1 : 10 HCl (1 L) aqueous solution until its pH ranged between 5 and 6 and then dried at 60 °C in vacuum for 12 h.

Preparation of free-standing rGOM

Certain amounts of GO (5, 10, 20, 30, 40, and 50 mg) were dispersed in 10 mL of DI water. Yellow homogeneous GO solutions of different concentrations were then obtained by ultrasonication for 2 h in a water bath sonicator. For free-standing GOM formation, the obtained GO solutions were vacuum-filtered through a filter membrane (Millipore, 50 mm, 0.22 μm pore size) for 1 h under positive pressure. Subsequently, the GOM on the filter membrane was transferred into an oven and dried at 60 °C for 40 min. The residue was then picked up and immersed in acetone for several seconds. The GOM was detached from the filter membrane support using tweezers. The as-prepared GOMs at varying amounts were reduced by HI at 100 °C for 1 h in an oil bath, washed several times with ethanol and DI water, and completed dried in a vacuum oven at 80 °C for 12 h. rGOMs were thus obtained and designated as rGOM-5, rGOM-10, rGOM-20, rGOM-30, rGOM-40, and rGOM-50 according to the amounts of GO used. The synthetic procedure for these samples is illustrated in Fig. 1.

Material characterization

The contents of carbon in the membrane materials were determined by an element analyzer (EA, VarioEL III). The powder X-ray diffraction (XRD) patterns of the samples were recorded by a Bruker D8 ADVANCE X-ray powder diffractometer using Cu Kα radiation ($\lambda = 0.15418$ nm) at a scanning rate of $0.02^\circ\ s^{-1}$ in the 2θ range from 10° to 70°. Scanning electron microscopy (SEM) images of the samples were measured by an FEI Quanta 400 ESEM-FEG (environmental scanning electron microscope-field emission gun) instrument with an accelerating voltage of 20 kV equipped with an X-ray energy dispersive spectrometer (EDS). The pore size distribution of the samples was obtained using nitrogen adsorption *via* Barrett–Joyner–Halenda (BJH) method. X-ray photoelectron spectrum (XPS) measurements were performed on a PHI-5400 electron spectrometer. Raman spectra were recorded by a dispersive Raman spectrometer (Nicolet, ALMEGA Company) with an excitation wavelength of 532 nm.

Electrochemical measurements

Electrochemical measurement was carried out at 25 °C using a coin-type cell (CR2025) with pure lithium foil as the counter and reference electrode. To test the electrochemical performance of the flexible lithium-ion electrodes, flexible free-standing rGOMs were cut into appropriate sizes smaller than the 14 mm-

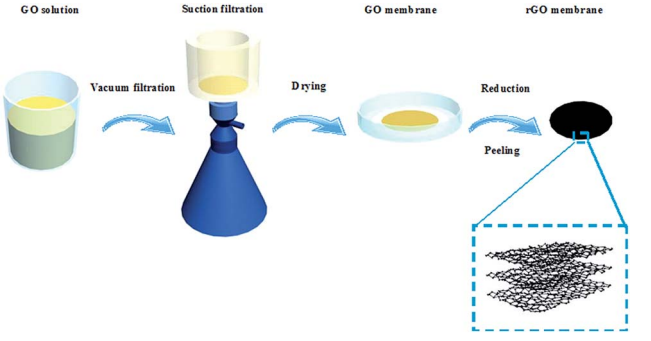

Fig. 1 Schematic illustration of the synthesis process for rGOM.

diameter Ni foam wafers and designed without using other carbon additives or binders. The rGOM pieces were then directly pressed onto the Ni foam at 20 MPa to achieve good contact between the active material and the Ni foam. The electrolyte solution was prepared by dissolving 1 M $LiPF_6$ in a mixture of dimethyl carbonate, diethyl carbonate, and ethylene carbonate (1 : 1 : 1 by volume), and the separator was a microporous polypropylene film. Cell assembly was carried out in an Ar-filled glovebox with moisture and oxygen concentrations below 1.0 ppm. Discharge–charge tests were performed using a LAND battery program-control test system (CT 2001A, Wuhan Jinnuo Electronic Co. Ltd. of China) in a cut-off voltage window of 0.005–3.0 V. Cyclic voltammetry (CV) was carried out on an electrochemical workstation (660D, CHI company, China) at a scan rate of 0.1 mV s^{-1} in the potential range of 0–3.0 V *vs.* Li/Li^+. Electrochemical impedance spectroscopy (EIS) was performed using the same electrochemical workstation over the frequency range of 0.01–100 kHz.

Results and discussion

Optical photographs of GOMs and rGOMs are shown in Fig. 2. All of the as-prepared free-standing GOMs show smooth surfaces with different colors. As the GO solution concentration increases, the color of the as-obtained GOMs darkens and changes from light brown to puce. This phenomenon indicates that the thickness of the GOMs increases gradually, which can also be confirmed by their transmittance spectra results (Fig. 3).

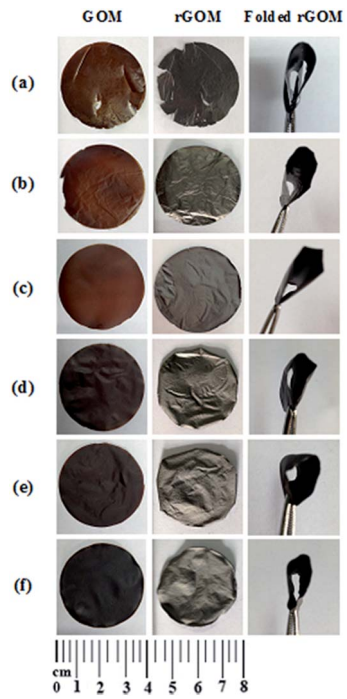

Fig. 2 Photographs of GOMs and rGOMs synthesized by using different concentration of GO solution: (a) 0.5 mg mL^{-1} GO and rGOM-5; (b) 1.0 mg mL^{-1} GO and rGOM-10; (c) 2.0 mg mL^{-1} GO and rGOM-20; (d) 3.0 mg mL^{-1} GO and rGOM-30; (e) 4.0 mg mL^{-1} GO and rGOM-40; (f) 5.0 mg mL^{-1} GO and rGOM-50.

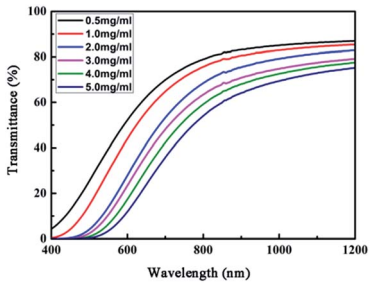

Fig. 3 Transmittance spectra of GOMs synthesized by using different concentration of GO solution.

As shown in Fig. 3, optical transparencies of the GOMs decrease with increasing membrane thickness. In contrast to the original GOMs, all of the rGOMs exhibit dark black coloration with a weak metallic luster on their surfaces and possess very flexible and coriaceous paper-like structures. After reduction by HI acid, most of the rGOMs, except rGOM-5, can be bent without damage. This result provides clear inference that rGOM synthesized from a low GO solution concentration is too fragile to form a stable membrane morphology.

The surface morphologies of the rGOMs were measured by SEM, and results are displayed in Fig. 4. Regardless of the amount of GO used for membrane formation, the final samples obtained all exhibit very similar characteristics. A large number of gossamer-like rGO sheets closely associate with one another to form a surface with curled and corrugated structures. The rGOMs cross-sectional morphologies were determined by SEM to measure their thicknesses (Fig. 5). The thinnest membrane can clearly be observed in Fig. 5(a), this membrane displays a thickness of 1.4 μm. With increasing GO concentration, the thickness of the related membranes increases gradually. Based on Fig. 5, the average thickness of each rGOM can be roughly calculated, and relevant results are shown in Table 1. The fracture edges indicate that a layer-by-layer stacking mode exists in all rGOMs and that the distance between these stacked "wavy" layers is approximately 100–200 nm.

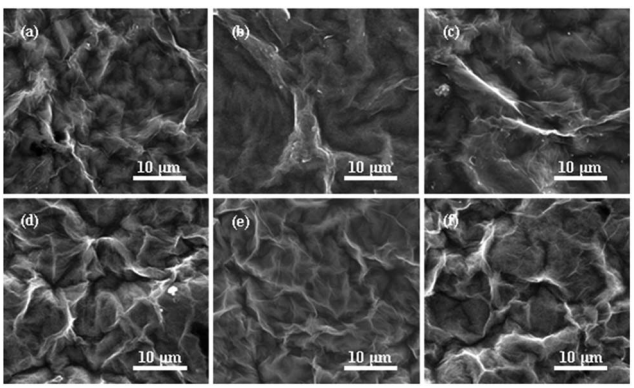

Fig. 4 SEM images of rGOMs synthesized by using different concentration of GO solution: (a) 0.5, (b) 1.0, (c) 2.0, (d) 3.0, (e) 4.0, and (f) 5.0 mg mL^{-1}.

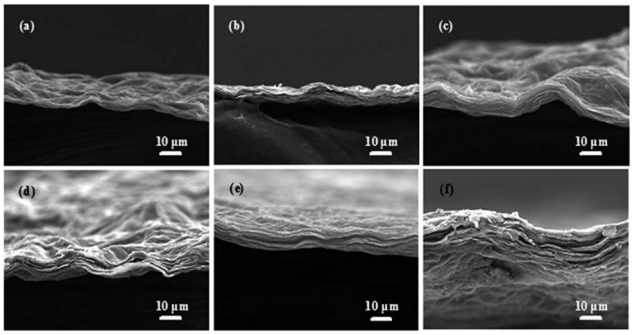

Fig. 5 SEM images of the cross-section view of rGOMs synthesized by using different concentration of GO solution: (a) 0.5, (b) 1.0, (c) 2.0, (d) 3.0, (e) 4.0, and (f) 5.0 mg mL^{-1}.

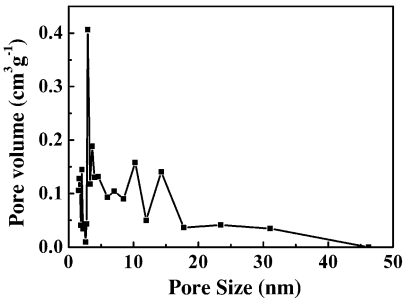

Fig. 6 The BJH pore size distribution of rGOM-10.

In order to investigate the pore structure of the rGOMs, a nitrogen isothermal adsorption technique was used. Because the pore size distributions for these membranes are similar to each other, here we only display the result of rGOM-10 as the example in Fig. 6. The Barrett–Joyner–Halenda (BJH) pore size distribution of rGOM-10 indicates the existence of micropores and mesopores. The total pore volume of rGO sheets is as high as 1.38 cm^3 g^{-1}, but the micropore volume is too small to be considered, revealing a very low micropore content. The average pore diameter is about 18.67 nm. This porosity structure of rGOMs can be very helpful for buffering the volume expansion during lithium insertion, which may contribute to a better cycling performance.

The XRD patterns of the synthesized GOMs and rGOMs are shown in Fig. 7. An obvious diffraction peak centered at 11.6° may be observed in the XRD patterns of the GOMs, this peak corresponds to a *d*-spacing of approximately 7.96 Å and is caused by interlamellar water trapped between hydrophilic GO sheets.[24] After chemical reduction treatments, the featured diffraction peaks then shift to ~24.3°. This result indicates that the interplanar spacing decreases to 3.75 Å.[25] No other detectable peaks from impurities are observed, which indicates the high purity of the synthesized GOMs and rGOMs.

Raman spectroscopy provides a powerful tool with which to determine the microstructure of carbon-based materials. Thus, Raman measurements were performed on the free-standing GOMs and rGOMs, as shown in Fig. 8. The Raman spectra of all of the GOMs display two prominent peaks: the D peak at 1335 cm^{-1}, which is attributed to edge planes and disordered structures, and the G peak at 1578 cm^{-1}, which corresponds to first-order scattering of the E_{2g} mode observed for sp^2 domains.[26–28] Compared with those of the GOMs, the Raman spectra of rGOMs also present both D and G bands (at 1330 and 1580 cm^{-1}, respectively). The I_D/I_G ratios embodied in the Raman spectra of rGOMs verify that significant graphitic regions exist within these reduced materials. The intensity ratio of the D and G bands in the spectrum of rGOM is 0.92, whereas that for GOM is obviously lower. This change suggests a decrease in the average size of in-plane sp^2 domains upon GO reduction as well as an increase in the edge planes and degree of disorder of the prepared rGO sheets.[26–31]

XPS studies were implemented to analyze the various elements, oxidation states, and purity of the synthesized materials. The XPS results of all six samples before and after reduction are extremely similar. Thus, for simplicity, the XPS results of the 1.0 mg mL^{-1} membranes are presented here as an example. Fig. 9(a) and (c) show the survey scan spectra of as-synthesized GOM-10 and rGOM-10. The presence of C1s (284.6 eV) and O1s (532 eV) can be observed in both GOM and rGOM. Oxygen functional groups in rGOM are substantially decreased by reduction, and the intensity of the C1s peak in rGOM is higher than that in GOM. High-resolution C1s peak in the XPS of rGOM proves that most oxygen-containing groups are effectively expelled during HI acid reduction. The C1s spectrum of GOM [Fig. 9(b)] shows that GOM comprises two main components arising from C–O (hydroxyl and epoxy, 286.5 eV) and C=C/C–C (284.6 eV) groups as well as a minor component from C=O (carbonyl, 288.3 eV) group.[30] After HI reduction, the hydroxyl and epoxy groups, which make up the majority of oxygen-containing groups in GOM, are nearly completely removed and C–C bonds become dominant, as shown by the single strong peak at 284.6 eV (C=C/C–C) and a small weak peak at 286.5 eV (C–O) in Fig. 9(d). Table 2 gives the carbon contents of the six rGOM samples, results clearly reflect the reduction degree of these membranes. Increasing the GO concentration, causes successive decreases in the carbon contents of the related rGOMs. This result can be ascribed to the reduction degree of the rGOMs, which directly affects the sample C/O ratio. The higher the GO concentration is, the thicker the rGOM becomes. When reduced by equal degrees, the thicker membrane will show a lower reduction degree and lower sample C/O ratio.

Table 1 The average thickness of rGOMs synthesized by using different concentration of GO solution

Sample	rGOM-5	rGOM-10	rGOM-20	rGOM-30	rGOM-40	rGOM-50
Average thickness (μm)	1.4	2.5	5.1	7.3	12.4	16.4

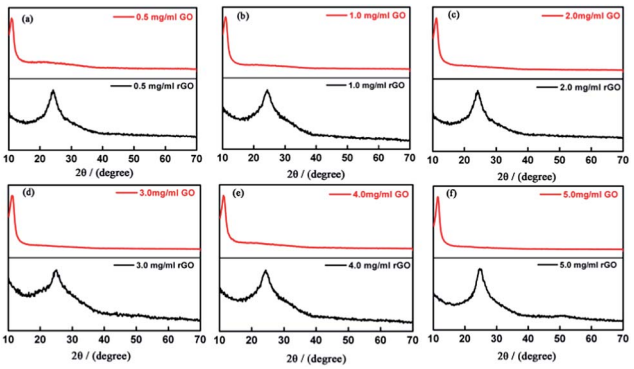

Fig. 7 XRD patterns of GOMs and rGOMs synthesized by using different concentration of GO solution: (a) 0.5 mg mL^{-1} GO and rGO-5; (b) 1.0 mg mL^{-1} GO and rGO-10; (c) 2.0 mg mL^{-1} GO and rGO-20; (d) 3.0 mg mL^{-1} GO and rGO-30; (e) 4.0 mg mL^{-1} GO and rGO-40; (f) 5.0 mg mL^{-1} GO and rGO-50.

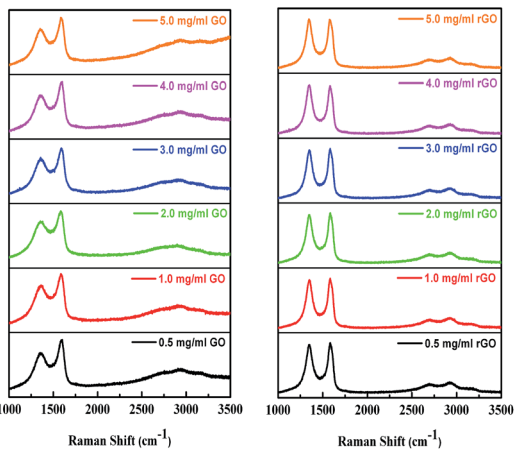

Fig. 8 Raman patterns of GOMs and rGOMs synthesized by using different concentration of GO solution.

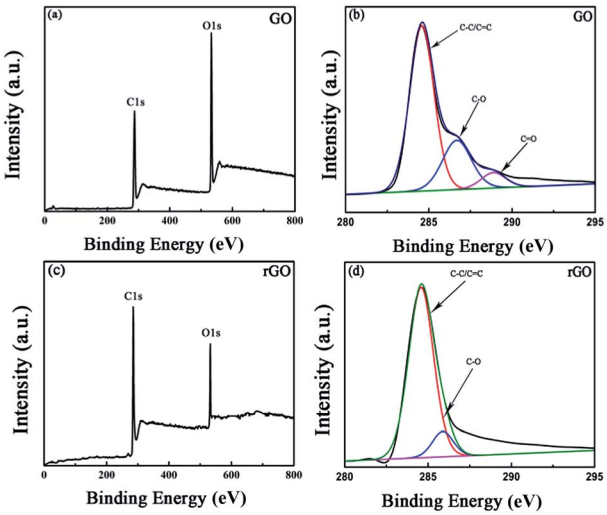

Fig. 9 X-ray photoelectron spectroscopy (XPS) of GOMs-10 and rGOMs-10. Survey spectra (a and c) and high-resolution core level spectra of C1s signal (b and d).

After successful synthesis of rGOMs with different thicknesses and reduction degrees, the electrochemical properties of the products as anode materials for LIBs were investigated and compared. EIS measurements were carried out in order to compare the conductivity of rGOM electrodes. In the equivalent circuit [Fig. 10(a)], a modified Randles equivalent circuit was incorporated to fit the data points. R_Ω and R_{ct} are the ohmic resistance (total resistance of the electrolyte, separator, and electrical contacts) and charge-transfer resistance, respectively. CPE is the constant phase-angle element involving double-layer capacitance, and W represents the Warburg impedance reflecting the solid-state diffusion of lithium ion into the bulk of the active materials. Fig. 10(b) compares the Nyquist plots of the rGOM anodes before the charge–discharge cycles. All of the anodes exhibit two distinct parts: a semicircle in the high-frequency range, which may be assigned to R_{ct}, and an inclined line in the low-frequency range, which represents W.[32] In general, the smaller the diameter of a semicircle, the lower the R_{ct} of an electrode. Based on Fig. 10(b), increasing the rGOM concentration causes the R_{ct} of the membranes to increase gradually. The lowest R_{ct} (smallest diameter of semicircle) is obtained from rGOM-5. This result is relevant to the thickness and reduction degree of the rGOMs.[33] On the one hand, by increasing the thickness of the rGOMs, the layer numbers of the rGO sheets increase [Fig. 5(a)–(f)]. Increases in the layer numbers of rGO sheets imply that migration of lithium ions and electrons in the vertical direction of the electrodes is prolonged. On the other hand, increases in rGOM thickness decreases in reduction degree and gradual increases in oxygen contents may be observed, as confirmed by the data in Table 2. These results suggest that after reduction, more oxygen functional groups may be observed in thick membranes than in thin membranes. Nevertheless, oxygen functionalities are not conducive to migration of lithium ions and electrons.[34] Therefore, the R_{ct} of the rGOMs gradually increases with increasing thickness.

The discharge–charge characteristics of the rGOMs were further researched. Fig. 11(a) presents the first three discharge–charge profiles of the rGOM-10 anode at 50 mA g^{-1} current density. An obvious difference can be observed between the voltage curves of the first and second discharge processes. In the first cycle, the potential profile shows an irreversible capacity at approximately 0.75 V, which is due to formation of a solid electrolyte interface (SEI) film on the surface of the rGOM electrode, electrolyte decomposition, and irreversible lithium ion reaction with residual oxygen-containing functional groups.[35,36] Furthermore, in the first discharge curve, the slope begins at approximately 2.8 V and exhibits large specific capacities below 0.5 V with no distinguishable plateaus. The capacity of the potential region lower than 0.5 V may be attributed to lithium intercalation into the rGO layers. The absence of a potential plateau below 0.5 V implies that the rGO sheets feature disordered stacking, which results in electrochemically and geometrically non-equivalent lithium ion sites. Capacities above 0.5 V may be ascribed to the faradaic

Table 2 The carbon contents in rGOMs synthesized by using different concentration of GO solution

Sample	rGOM-5	rGOM-10	rGOM-20	rGOM-30	rGOM-40	rGOM-50
Carbon content (%)	77.5	77.3	77.2	71.0	69.8	60.3

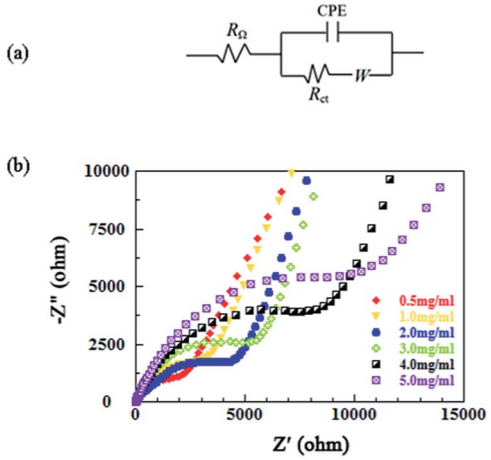

Fig. 10 Electrochemical impedance spectroscopy (EIS) measurements. (a) Modified Randles equivalent circuit used to fit EIS data. (b) Comparison of the rGOMs electrodes.

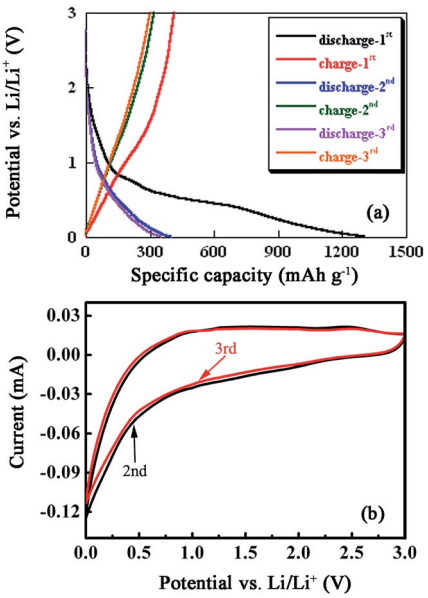

Fig. 11 (a) The first three discharge–charge profiles of the synthesized rGOM-10 electrode at the current density of 50 mA g^{-1}, (b) the second and third CV curves of the synthesized rGOM-10.

capacitance on the surface or edge sites of the rGO sheets.[37] No obvious plateaus are observed in the second and third discharge–charge profiles. The cyclic voltammogram (CV) shapes are similar for all rGOM electrodes, hence, only the CV curves of rGOM-10 are considered in the present discussion for analysis. Fig. 11(b) shows the CV curves of the rGOM-10 electrode in the second and third cycles, these curves were recorded at a scan rate of 0.5 mV s^{-1} between 0 and 3.0 V. The CV curves match the discharge–charge voltage profiles well [Fig. 11(a)], they exhibit good reproducibility and nearly coincide in shape, which indicate the high reversibility of the electrode.

The long-term cyclic performance and capacity retention of the rGOM electrodes over 1000 cycles are shown in Fig. 12. It is observed that the rGOM-5 electrode displays the highest capacity within the first 200 cycles [Fig. 12(a)]. However, its capacity fades quickly over the following cycles. A poor capacity of ~60 mA h g^{-1} can only be obtained at the 1000th cycle (capacity retention: 29%). This result implies that this electrode has unstable electrochemical performance. Rapid reductions in capacity during long cycles may limit the practical use of this material.[38] The highest initial capacity of rGOM-5 electrode may be ascribed to its minimal R_{ct} (*i.e.*, highest conductivity) [Fig. 10(b)]. Unfortunately, this membrane is very thin and fragile, hence, the integrity of the electrode structure may be destroyed during repeated intercalation–de-intercalation processes, thereby leading to a rapid drop in its ability to store lithium ions. By contrast, all other electrodes from rGOM-10 to rGOM-50 perform well during the long-cycle life test and exhibit good cyclic retention after the initial 20 cycles. For example, over 20 cycles, the reversible discharge capacities of rGOM-10, rGOM-20, rGOM-30, rGOM-40, and rGOM-50 are approximately 174, 143, 86, 49, and 7 mA h g^{-1}, respectively.

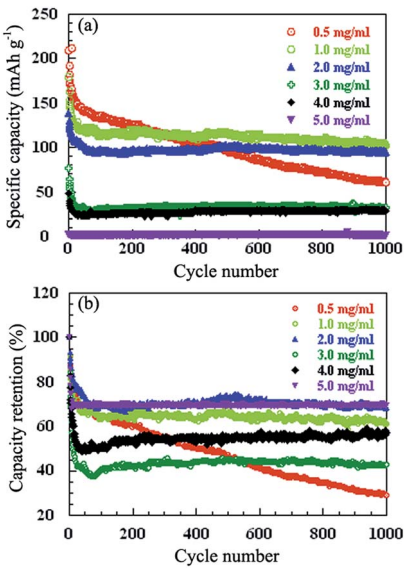

Fig. 12 (a) The cycle performance and (b) capacity retention of rGOMs electrodes for 1000 cycles at the current density of 200 mA g^{-1}.

After 1000 cycles, these rGOM cells maintain discharge capacities of 123 (rGOM-10), 94 (rGOM-20), 38 (rGOM-30), 28 (rGOM-40), and 6 mA h g^{-1} (rGOM-50). The capacity retentions of rGOMs anodes at the 1000th cycle are 62%, 68%, 43%, 53% and 69%, respectively [Fig. 12(b)], indicating a relatively slow capacity fading of these anodes over long-term cycles compared with rGOM-5. As the rGOMs thicknesses increase, their capacities decrease in the order of rGOM-10 > rGOM-20 > rGOM-30 > rGOM-40 > rGOM-50. Despite the capacity retention of rGOM-50 is superior to other reported rGOM anodes, its capacity is the lowest. The specific capacities and capacity retentions of rGOM-30 and rGOM-40 are very low, so all of them (rGOM-30, rGOM-40 and rGOM-50) can be ignored. Therefore, among the rGOM electrodes tested, rGOM-10 and rGOM-20, with thicknesses of 2.5 and 5.1 μm, are the most suitable for practical applications.

The rate capabilities of the rGOM electrodes at various current densities of 50, 100, 200, 400, and 800 mA g^{-1} are displayed in Fig. 13. The average reversible capacities of the electrodes at different current densities are given in Fig. 14. Based on these two figures, the rGOM-5 electrode displays the highest discharge–charge capacity among all rGOM electrodes studied at every tested current density. However, the intercalation–de-intercalation process of lithium ion at each current density is held for such a relatively short time (10 cycles). Considering the long-term cyclic performance of the electrodes, the capacity retention of rGOM-5 is the poorest among the samples. Thus, rGOM-5 is not the best choice for LIBs. The order of the rate capabilities of the other electrodes, without considering rGOM-5, is similar to that of their cyclic performance, that is, rGOM-10 > rGOM-20 > rGOM-30 > rGOM-40 > rGOM-50. This phenomenon demonstrates that among rGOMs under study, the rGOM-10 and rGOM-20 electrodes are the best choice for practical application.

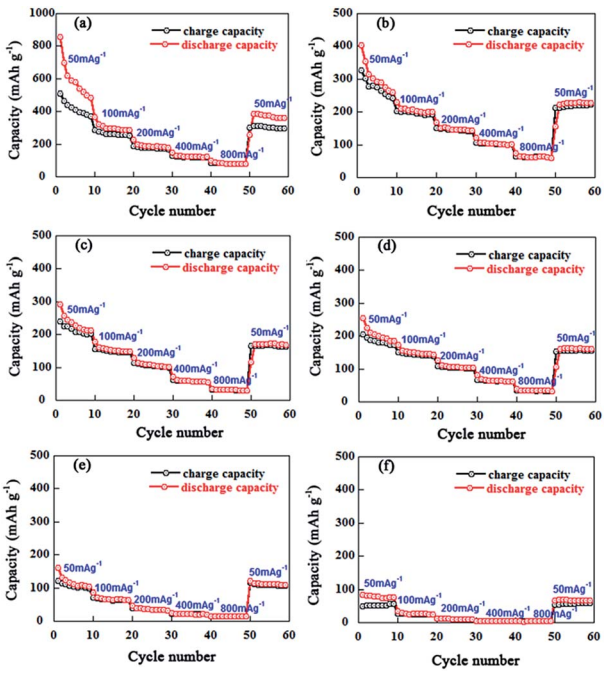

Fig. 13 The rate performance of rGOMs electrodes at different current density: (a) 0.5, (b) 1.0, (c) 2.0, (d) 3.0, (e) 4.0, and (f) 5.0 mg mL^{-1}.

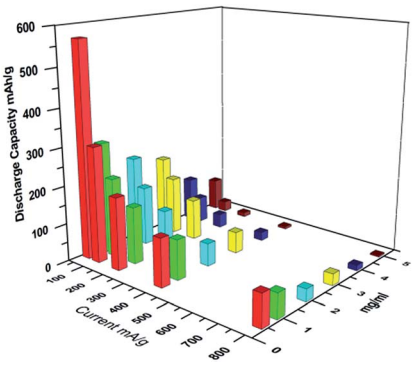

Fig. 14 The average discharge capacities for rGOMs electrodes at various current densities.

Although the capacities of the as-prepared rGOM electrodes show a certain changing regularity as their thickness changes, they are still limited by their low specific capacities. In this work, the best electrochemical performance among the rGOM electrodes tested is realized on rGOM-10 based on the fact that every electrode can steadily exert their capacities. A high reversible discharge capacity of 228 mA h g^{-1} is obtained when the current density is reduced back to 50 mA g^{-1} after 60 cycles. The rGOM-10 electrode shows an excellent discharge capacity of 123 mA h g^{-1} and good capacity retention of 62% after 1000 charge–discharge cycles at 200 mA g^{-1}. Considering their advantages of a simple two-step preparation method and good stability to maintain capacity, rGOM electrodes may be considered promising materials in the field of energy storage. The high electrical conductivity of rGOM electrodes is expected to lead to significant benefits when the electrodes are used as electrode current collectors in future applications.

Conclusions

Free-standing rGOMs with different thicknesses and carbon contents were synthesized *via* a simple two-step method to achieve low-cost and eco-friendly mass production of rGOMs, especially rGOM-10, as efficient electrode materials for LIBs. SEM results showed that the thickness of the rGOMs increases with increasing rGO solution concentration. In anode tests for LIBs, rGOM-10 exhibited the best electrochemical performance among the rGOM electrodes tested. This result is mainly attributed to the following: (1) a flexible and coriaceous paper-like structure, which maintains electrode integrality during cycles, resulting in a large reversible capacity and good cycling stability; (2) an appropriate thickness consisting of a small number of rGOM layers, which causes the distances for lithium ion diffusion and electron transfer to shorten; and (3) a proper reduction degree, which produces an appropriate C/O ratio and decreases the R_{ct}.

Acknowledgements

This work was supported by the financial supports of the National Natural Science Foundation of China (no. 21061130551), and the Xi'an Industrial Technology Innovation Project-technology transfer promoting program (no. CXY1438-7).

Notes and references

1 J. Liu, J. G. Zhang, Z. G. Yang, J. P. Lemmon, C. Imhoff, G. L. Graff, L. Y. Li, J. Z. Hu, C. M. Wang, J. Xiao, G. Xia, V. V. Viswanathan, S. Baskaran, V. Sprenkle, X. L. Li, Y. Y. Shao and B. Schwenzer, *Adv. Funct. Mater.*, 2013, **23**, 929–946.
2 J. M. Tarascon and M. Armand, *Nature*, 2001, **414**, 359–367.
3 J. Vetter, P. Novak, M. R. Wagner, C. Veit, K. C. Moller, J. O. Besenhard, M. Winter, M. Wohlfahrt-Mehrens, C. Vogler and A. Hammouched, *J. Power Sources*, 2005, **147**, 269–281.
4 X. Y. Xue, Z. H. Chen, L. L. Xing, S. Yuan and Y. J. Chen, *Chem. Commun.*, 2011, **47**, 5205–5207.
5 L. W. Ji, Z. Lin, M. Alcoutlabi and X. W. Zhang, *Energy Environ. Sci.*, 2011, **4**, 2682–2699.
6 P. C. Lian, X. F. Zhu, S. Z. Liang, Z. Li, W. S. Yang and H. H. Wang, *Electrochim. Acta*, 2010, **55**, 3909–3914.
7 A. K. Geim and K. S. Novoselov, *Nat. Mater.*, 2007, **6**, 183–191.
8 S. Stankovich, D. A. Dikin, G. H. B. Dommett, K. M. Kohlhaas, E. J. Zimney, E. A. Stach, R. D. Piner, S. B. T. Nguyen and R. S. Ruoff, *Nature*, 2006, **442**, 282–286.
9 C. G. Lee, X. D. Wei, J. W. Kysar and J. Hone, *Science*, 2008, **321**, 385–388.
10 R. Z. R. R. Rosdin, F. Ahmad, N. M. Ali, S. W. Harun and H. Arof, *Chin. Opt. Lett.*, 2014, **12**, 091404–091408.
11 Z. S. Wu, W. C. Ren, L. Xu, F. Li and H. M. Cheng, *ACS Nano*, 2011, **7**, 5463–5471.
12 D. Li and R. B. Kaner, *Science*, 2008, **320**, 1170–1171.
13 C. Rizza, E. Palange and A. Ciattoni, *Photonics Res.*, 2014, **2**, 121–125.
14 J. S. Xue and J. R. Dahn, *J. Electrochem. Soc.*, 1995, **142**, 3668–3677.
15 D. Y. Pan, S. Wang, B. Zhao, M. H. Wu, H. J. Zhang, Y. Wang and Z. Jiao, *Chem. Mater.*, 2009, **21**, 3136–3142.
16 R. Yazami and M. Deschamps, *J. Power Sources*, 1995, **54**, 411–415.
17 S. H. Ha, Y. S. Jeong and Y. J. Lee, *ACS Appl. Mater. Interfaces*, 2013, **5**, 12295–12303.
18 X. Zhao, C. M. Hayner, M. C. Kung and H. H. Kung, *ACS Nano*, 2011, **5**, 8739–8749.
19 H. Gwon, H. S. Kim, K. U. Lee, D. H. Seo, Y. C. Park, Y. S. Lee, B. T. Ahn and K. Kang, *Energy Environ. Sci.*, 2011, **4**, 1227–1283.
20 Z. L. Wang, D. Xu, H. G. Wang, Z. Wu and X. B. Zhang, *ACS Nano*, 2013, **7**, 2422–2430.
21 F. Liu, S. Y. Song, D. F. Xue and H. J. Zhang, *Adv. Mater.*, 2012, **24**, 1089–1094.
22 M. S. Xu, D. Fujita, J. H. Gao and N. Hanagata, *ACS Nano*, 2010, **4**, 2937–2945.
23 W. S. Hummers and R. E. Offeman, *J. Am. Chem. Soc.*, 1958, **80**, 1339.
24 M. Kim, D. Y. Kim, Y. K. Kang and O. O. Park, *RSC Adv.*, 2015, **5**, 3299–3305.
25 S. J. Park, J. H. An, I. Jung, D. P. Richard, S. J. An, X. S. Li, A. Velamakanni and R. S. Ruoff, *Nano Lett.*, 2009, **9**, 1593–1597.
26 K. N. Kudin, B. Ozbas, H. C. Schniepp, R. K. Prud'homme, I. A. Aksay and R. Car, *Nano Lett.*, 2008, **8**, 36–41.
27 A. C. Ferrari and J. Robertson, *Phys. Rev. B: Condens. Matter Mater. Phys.*, 2000, **61**, 14095.
28 M. A. Pimenta, G. Dresselhaus, M. S. Dresselhaus, L. G. Cancado, A. Jorioa and R. Saito, *Phys. Chem. Chem. Phys.*, 2007, **9**, 1276–1290.
29 F. Tuinstra and J. L. Koenig, *J. Chem. Phys.*, 1970, **53**, 1126–1130.
30 S. Stankovich, D. A. Dikin, R. D. Piner, K. A. Kohlhaas, A. Kleinhammes, Y. Jia, Y. Wu, S. T. Nguyen and R. S. Ruoff, *Carbon*, 2007, **45**, 1558–1565.
31 G. Wang, J. Yang, J. Park, X. Gou, B. Wang, H. Liu and J. Yao, *J. Phys. Chem. C*, 2008, **112**, 8192–8195.
32 D. Zhang, Y. J. Mai, J. Y. Xiang, X. H. Xia, Y. Q. Qiao and J. P. Tu, *J. Power Sources*, 2012, **217**, 229–235.
33 I. Jung, D. A. Dikin, R. D. Piner and R. S. Ruoff, *Nano Lett.*, 2008, **8**, 4283–4287.
34 Z. B. Lei, L. Lu and X. S. Zhao, *Energy Environ. Sci.*, 2012, **5**, 6391–6399.
35 D. Aurbach, *J. Power Sources*, 2000, **89**, 206–218.
36 W. B. Xing and J. R. Dahn, *J. Electrochem. Soc.*, 1997, **144**, 1195–1201.
37 E. J. Yoo, J. Kim, E. Hosono, H. S. Zhou, T. Kudo and I. Honma, *Nano Lett.*, 2008, **8**, 2277–2282.
38 L. Zou, L. Gan, R. Lv, M. X. Wang, Z. H. Huang, F. Y. Kang and W. C. Shen, *Carbon*, 2011, **49**, 89–95.